

## Original Articles

# The impact of impervious surface expansion morphology on ecosystem services and thresholds in the Haihe River basin

Yang Gu<sup>a</sup>, Yujia Chen<sup>a</sup>, Dongdong Yang<sup>a,\*</sup>, Xin Zhao<sup>b,c,\*</sup>, Shunqi Pan<sup>d</sup>

<sup>a</sup> School of Architecture, Tianjin University, Tianjin 300072, China

<sup>b</sup> State Key Laboratory of Hydraulic Engineering Intelligent Construction and Operation, Tianjin University, Tianjin 300072, China

<sup>c</sup> School of Civil Engineering, Tianjin University, Tianjin 300072, China

<sup>d</sup> School of Engineering, Cardiff University, Queen's Buildings, The Parade, Cardiff CF24 3AA, United Kingdom

## ARTICLE INFO

## Keywords:

Ecosystem services  
Impervious surface areas  
Nonlinear relationships  
Basin planning  
Sustainable development

## ABSTRACT

The rapid expansion of impervious surface areas (ISA) has a profound impact on basin ecosystem services (ES). However, the relationship between impervious surface expansion morphology (ISEM) and ES remains insufficiently studied. This study focused on the Haihe River Basin (HRB) and first quantified ISEM from three dimensions i.e. patch scale, shape complexity, and spatial aggregation. The InVEST model was then employed to assess ES, including habitat quality, carbon storage, water yield, and soil conservation, followed by the calculation of comprehensive ecosystem service (CES). Subsequently, GeoDetector and restricted cubic spline were employed to analyze the drivers, interactions, and threshold effects of ISEM on CES. Finally, an analysis of variance was conducted to identify ISEM profiles for regions with different CES levels, offering a basis for basin zoning and planning. The results indicated that: (1) All ISEM indicators had a significant impact on CES. Notably, during the period from 2002 to 2022, the euclidean nearest-neighbor distance mean (ENN\_MN) showed the largest influence on CES, with q-values of 0.601, 0.586, and 0.561, respectively; (2) Except for mean shape index (SHAPE\_MN), other ISEM indicators showed significant nonlinear relationships with CES ( $p < 0.001$ ), with their impact on CES changing after exceeding certain thresholds; and (3) ISEM profiles exhibited contrasting differences between regions with high and low CES.

## 1. Introduction

With the acceleration of global urbanization, basin ecosystems are facing unprecedented challenges (Zhang et al., 2021). Impervious surface areas (ISA), as one of the core features of urbanization, primarily involves built-up areas, roads, plazas, and parking lots, with surfaces typically covered by impermeable materials such as tar, concrete, and asphalt. The continuous expansion of ISA disrupts matter and energy exchanges between soil and the atmosphere (Wang et al., 2024), leading to habitat degradation, soil erosion, and alterations in carbon and water cycles (Li & Liu, 2019; Xiao et al., 2020), thereby affecting basin ecosystem services (ES). ES are defined as ecological attributes, functions, or processes that directly or indirectly enhance human well-being (Costanza et al., 1997) and are categorized into provisioning, regulating,

supporting, and cultural services (Cord et al., 2017). Therefore, quantifying the extent and spatial distribution of ISA expansion is fundamental to assessing its impact on ES and essential for developing effective management strategies.

Advances in remote sensing technology and data processing capabilities have provided higher-resolution imagery and more accurate monitoring methods for ISA research (Chen et al., 2020; Liu et al., 2020). Currently, the measurement of ISA expansion primarily focuses on area, change rate, and spatial distribution (Deng & Zhu, 2020; Gong et al., 2020; Gui et al., 2024). In addition, some researchers have classified expansion patterns into three types (edge expansion, internal infill, and leapfrog expansion) based on the spatial relationship between newly added and existing ISA patches, and explored their different impacts on ES (Zhong et al., 2023). However, existing research generally focuses on

**Abbreviations:** CA, class area; CES, comprehensive ecosystem service; COHESION, patch cohesion index; ENN\_MN, euclidean nearest-neighbor distance mean; ES, ecosystem services; HRB, the Haihe River Basin; ISA, impervious surface areas; ISEM, impervious surface expansion morphology; NP, number of patches; PAFRAC, perimeter-area fractal dimension; SHAPE\_MN, mean shape index.

\* Corresponding authors.

E-mail addresses: [guyanggy520@163.com](mailto:guyanggy520@163.com) (Y. Gu), [ydongdong0308@163.com](mailto:ydongdong0308@163.com) (D. Yang), [xin.zhao@tju.edu.cn](mailto:xin.zhao@tju.edu.cn) (X. Zhao), [PanS2@cardiff.ac.uk](mailto:PanS2@cardiff.ac.uk) (S. Pan).

<https://doi.org/10.1016/j.ecolind.2025.113493>

Received 24 December 2024; Received in revised form 31 March 2025; Accepted 14 April 2025

Available online 26 April 2025

1470-160X/© 2025 The Author(s). Published by Elsevier Ltd. This is an open access article under the CC BY-NC-ND license (<http://creativecommons.org/licenses/by-nc-nd/4.0/>).

single-dimensional ISA indicators (Ma et al., 2021), lacking multi-dimensional assessments of ISA spatial expansion morphology, particularly in quantifying critical landscape features such as shape complexity and spatial aggregation (Xu et al., 2023).

In recent years, the impact of urbanization on ES has attracted widespread attention (Qiu et al., 2024; Ren et al., 2022; Zheng et al., 2024). The impact of urbanization on ES is often assessed using multiple linear regression analysis to identify relationships between factors, GeoDetector to analyze spatial heterogeneity, geographically weighted regression to account for the influence of factors at different geographical locations, and spatial autocorrelation to measure the distribution characteristics and interrelationships of spatial data (Fang et al., 2024; Hou et al., 2020; Xia et al., 2023). These analyses provide significant theoretical support and empirical evidence for understanding the impact of urbanization on ES, but they fall short in capturing the complex nonlinear relationship between them. Ecosystems have critical points where even minor changes in external or internal factors can trigger significant shifts, affecting their ability to provide ES (Livina & Lenton, 2007; Scheffer et al., 2012). This transition point, known as a threshold, marks a change in the relationship between ecosystem state and its drivers (Peng et al., 2017). In nonlinear research, researchers typically employ models such as curve regression, piecewise regression, and threshold regression to reveal critical points and threshold effects, thereby gaining a holistic understanding of the complex interactions between variables (Hong et al., 2024; Li et al., 2022; Peng et al., 2017; Ran et al., 2023). For instance, Peng et al. (2017) employed piecewise linear regression to analyze the impact of urbanization on ES, identifying thresholds for population and economic urbanization. Ran et al. (2023) used threshold regression to reveal that population and land urbanization exhibit an inverted U-shaped relationship with carbon storage, while land urbanization shows a U-shaped relationship with food production. Therefore, nonlinear analysis can effectively reveal complex trends, contributing to a deeper understanding of the relationship between urbanization and ecosystems. Although ISA is considered an important indicator of urbanization and ecological environment, the extent to which its expansion morphology impacts ES and their nonlinear threshold relationships remains unclear.

Policies, through regulating land use and resource allocation, have a significant impact on the distribution patterns of ISA and ES (Deng et al., 2023; Ren et al., 2024). Socioeconomic development-driven policies often accelerate the expansion of built-up areas, leading to large-scale reductions in natural habitats and potentially triggering systematic degradation of ES (Reader et al., 2022). To address this issue, many countries have implemented ecological area control policies, such as designating ecological protection red lines and promoting ecological restoration projects, which have effectively enhanced the supply capacity of ES (He et al., 2025; Samuel et al., 2023). Thus, policies play a dual role in regulating the balance between ISA expansion and ES, as they can both exacerbate ecological pressure and promote ecological restoration (Mao et al., 2019; Yang et al., 2024). In recent years, China has faced increasingly severe water scarcity and ecological degradation, which have significantly constrained sustainable basin development (Wang et al., 2014). To deal with this challenge, the Chinese government has actively advanced basin ecological protection and management during the 14th Five-Year Plan period (2021–2025) (National Development and Reform Commission, 2021; Ministry of Ecology and Environment, 2023). As one of the key river basins in the 14th Five-Year Plan, the Haihe River Basin (HRB) is typically representative due to its rapid urbanization and increasingly severe ecological and environmental pressures (Bin et al., 2024). Therefore, taking the HRB as a case study, we developed an ISA planning framework based on comprehensive ecosystem service (CES) zoning. This framework summarized the impervious surface expansion morphology (ISEM) profiles of regions with different CES levels and integrated critical thresholds, thereby providing targeted planning recommendations for different zones. It aims to coordinate urbanization with ecological protection, achieving

sustainable development.

The main objectives of this study are: (1) to analyze the spatiotemporal distribution of ISEM and ES in the HRB from 2002 to 2022; (2) to explore the drivers, interactions, and threshold effects of ISEM on the spatial differentiation of CES; and (3) to identify the ISEM profiles of regions with different CES levels and propose planning recommendations based on critical thresholds. This study not only provides scientific rationale for ecological protection and management in the HRB, but also offers valuable insights for sustainable development in other river basins.

## 2. Methods and materials

### 2.1. Study area

HRB is located in North China (112°–120° E, 35°–43° N), covering an area of approximately 320,000 km<sup>2</sup>, and is one of the seven major river basins in China (Xu et al., 2014). The topography of the entire basin is characterized by a northwest-high and southeast-low gradient, with the highest point at 3,061 m (Ling et al., 2022). HRB has an annual average temperature ranging from 1.5 to 14 °C, an annual average relative humidity of 50 % to 70 %, and an average annual precipitation of 539 mm, classifying it as a semi-humid to semi-arid region (He et al., 2015). HRB spans eight provincial-level administrative regions and encompasses the Beijing-Tianjin-Hebei urban agglomeration, which holds significant political and economic importance in China (Ling et al., 2022). However, rapid urbanization has led to multiple environmental pressures in the HRB, including water resource over-exploitation, habitat fragmentation, and soil erosion, which severely constrain its sustainable development (Bin et al., 2024).

### 2.2. Data collection

The land use data for the HRB in 2002, 2012, and 2022 are derived from the 30-meter resolution China land cover dataset (CLCD) (<http://www.ncdc.ac.cn>). The dataset was developed on the Google Earth Engine platform using 335,709 Landsat images. It integrates training samples extracted from the China Land Use/Cover Dataset (CLUD), Google Earth imagery, and Google Maps, and categorizes land use into nine types: cropland, forest, shrub, grassland, water, snow/ice, barren, impervious, and wetland (Yang & Huang, 2021). Additionally, data on annual precipitation, evapotranspiration, digital elevation model, and root-limiting layer depth is provided in Appendix A, Table A.1.Fig. 1

### 2.3. Methodologies

#### 2.3.1. Planning framework

This study developed a comprehensive planning framework. Based on the analysis of the impact of ISEM on CES and its threshold effects, the framework incorporated the critical thresholds of ISEM and CES into urban planning considerations. It aimed to provide scientifically sound ISA planning recommendations for regions with different CES levels, thereby enhancing ES and promoting their sustainable development. The planning framework consisted of four steps, as shown in Fig. 2.

#### 2.3.2. Calculation of ISEM

For the calculation of ISEM, this study selected six indicators across three dimensions: patch scale, shape complexity, and spatial aggregation. These indicators, which were verified through collinearity diagnostics ( $VIF < 10$ ), include class area (CA), number of patches (Liu et al.), mean shape index (SHAPE\_MN), perimeter-area fractal dimension (PAFRAC), patch cohesion index (COHESION), and euclidean nearest-neighbor distance mean (ENN\_MN). Detailed formulas are provided in Appendix A. Using Fragstats 4.2 software and the 8-neighborhood rule, the study conducted batch calculations for the six ISEM

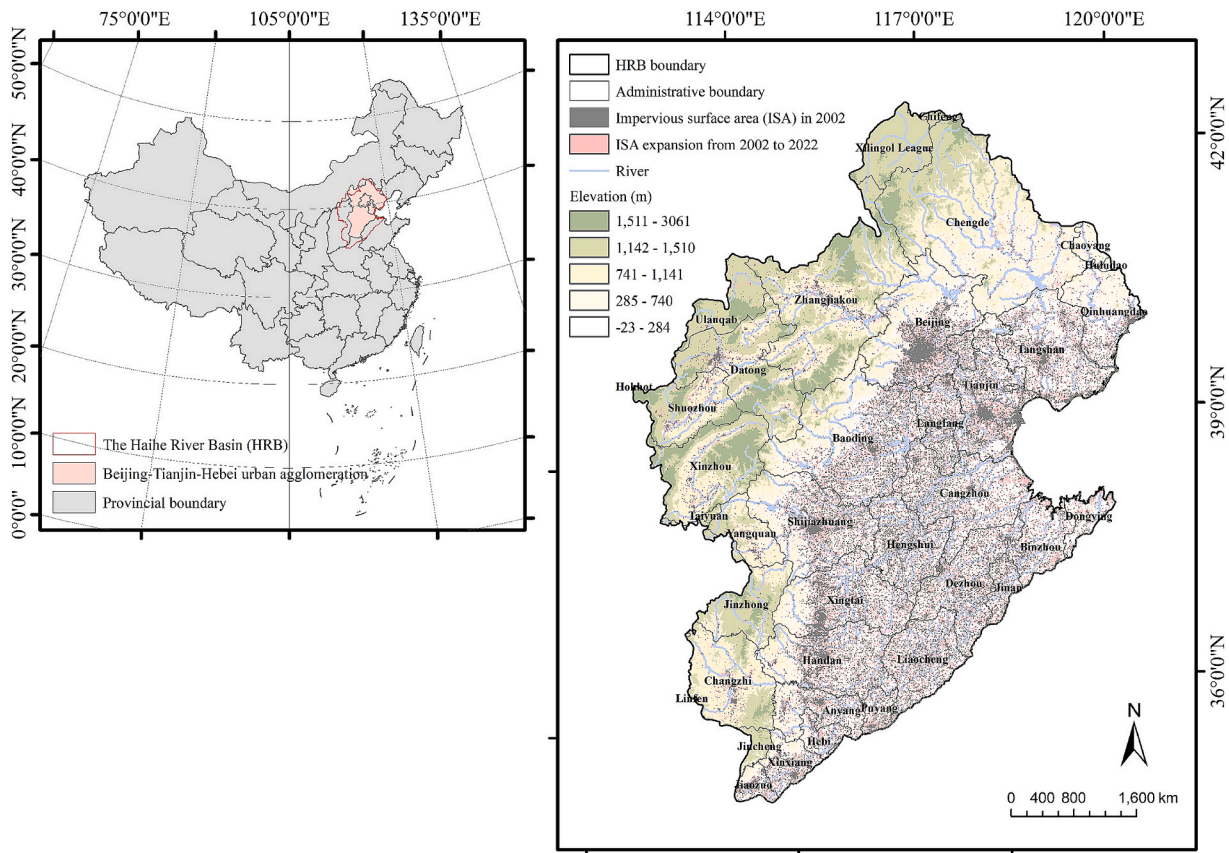


Fig. 1. Overview of the research area.

indicators across the HRB for the years 2002, 2012, and 2022.

### 2.3.3. Assessment of ES and CES

The InVEST model is widely used to assess ecosystem service functions, supporting ecosystem management and decision-making. The advantage of the InVEST model lies in its modular design and spatially explicit analysis capabilities, which allow for the quantification of multiple ES and the provision of intuitive spatial distribution maps, making it easier for decision-makers to understand and apply. In this study, the InVEST (version 3.14.2) model was employed to assess habitat quality, carbon storage, water yield, and soil conservation in the HRB for the years 2002, 2012, and 2022. The reliability of the output results was validated through model calibration and sensitivity analysis. Based on these results, CES was further calculated.

#### (1) ES

Habitat quality reflects the ability of ecosystems to sustain biodiversity. The habitat quality module integrates land use data and biodiversity threats to generate habitat quality maps. The formula is as follows:

$$Q_{ij} = H_j \left( 1 - \left( \frac{D_{ij}^z}{D_{ij}^z + k^z} \right) \right) \quad (1)$$

where  $Q_{ij}$  is the habitat quality of grid cell  $i$  with land use type  $j$ ,  $D_{ij}^z$  is the total threat level, and  $H_j$  is the habitat suitability. The parameter  $z$  is set to 2.5, and  $k$  is the half-saturation constant.  $Q_{ij}$  ranges from 0 to 1, with higher values indicating better quality.

Carbon storage represents one of the core functions of ES in regulating the global climate. The carbon storage module estimates the carbon stored in current land use types by accounting for four primary carbon pools: aboveground biomass, belowground biomass, soil, and dead matter. The formula is as follows:

$$CS = C_{a,i} + C_{b,i} + C_{s,i} + C_{d,i} \quad (2)$$

where CS represents the carbon density of grid cell  $i$ , and  $C_{a,i}$ ,  $C_{b,i}$ ,  $C_{s,i}$  and  $C_{d,i}$  denote the carbon densities of aboveground biomass, belowground biomass, soil, and dead matter, respectively.

Water yield is a crucial ecological indicator for assessing water resource availability and sustainability. The water yield module, based on the Budyko theory, establishes a relationship between the ratio of actual evaporation to precipitation and potential evapotranspiration. The formula is as follows:

$$WY_{ij} = \left( 1 - \frac{AET_{ij}}{P_{ij}} \right) \cdot P_{ij} \quad (3)$$

where  $WY_{ij}$  is the annual water yield,  $P_{ij}$  the annual average rainfall, and  $AET_{ij}$  the actual annual average evapotranspiration for grid cell  $i$  with land use type  $j$ .

Soil conservation is an important function for maintaining land productivity and ecosystem stability. The soil conservation module, based on the Universal Soil Loss Equation, calculates soil conservation using data such as topography, climate, vegetation, and land management. The formula is as follows:

$$\begin{aligned} RKLS &= R \times K \times LS \\ RUSLE &= R \times K \times LS \times C \times P \\ SC &= RKLS - RUSLE \end{aligned} \quad (4)$$

where RKLS represents potential soil erosion, RUSLE represents actual soil erosion, and SC represents actual soil conservation.  $R$  is the rainfall erosivity,  $K$  is the soil erodibility,  $LS$  is the slope length-gradient factor, where  $L$  is the slope length and  $S$  is the slope gradient,  $C$  is the cover-management factor, and  $P$  is the support practice factor.

#### (2) CES

CES is calculated to assess the overall level of ES in each city of the

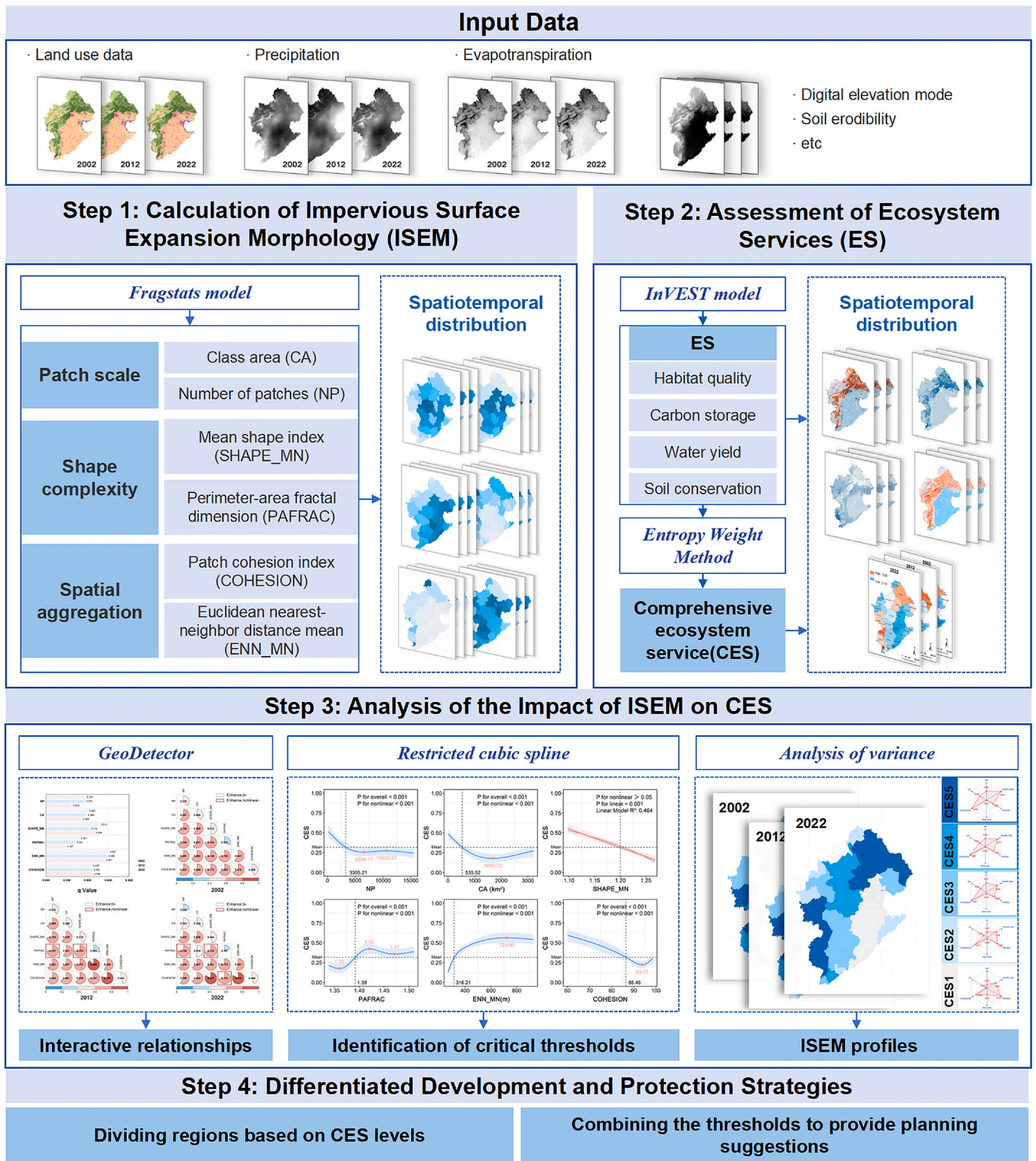


Fig. 2. Planning framework.

HRB. First, each ES is normalized, and then the entropy weight method is applied to determine the weights. Finally, CES is obtained by summing the weighted values of all ES (Ding et al., 2021).

$$CES_j = \sum_{i=1}^m \omega_i s_{ij} \quad (5)$$

where  $CES_j$  represents the value of CES in the  $j$  th year,  $\omega_i$  is the weight

of the  $i$  th ES, and  $s_{ij}$  signifies the standardized value for the  $i$  th ES in the  $j$  th year.

#### 2.3.4. Analysis of the impact of ISEM on CES

##### (1) GeoDetector.

GeoDetector is a statistical method based on spatial heterogeneity analysis, using the q-value to quantify the explanatory power of factors

on the dependent variable, and the specific formula can be found in Appendix A (Wang & Xu, 2017). Its advantage lies in not relying on linear assumptions, enabling effective detection of interactions between variables. The interaction detection module evaluates whether the combined effect of factors  $X_1$  and  $X_2$  enhances, weakens, or remains independent in explaining the dependent variable. The study utilized the factor detection and interaction detection modules in GeoDetector to analyze the drivers behind the spatial differentiation of ISEM on CES and the interactions among these factors.

(2) Restricted cubic splines.

Restricted cubic splines are a nonlinear regression method based on cubic spline functions, widely used to model nonlinear relationships between predictor variables and response variables (Hong et al., 2024; Li et al., 2022). Unlike traditional regression models, restricted cubic splines do not require predefined functional forms. Instead, they transform independent variables into cubic spline functions, flexibly capturing trends across different intervals. Additionally, restricted cubic splines imposes constraints on the spline functions, effectively preventing overfitting and ensuring model stability at extreme values (Bhaskaran et al., 2018; Dahlgren et al., 2011). This method demonstrates significant advantages in identifying threshold effects, enabling more precise detection of critical transition points between ES and their driving factors.

In this study, the “rms” package in R was used to implement the restricted cubic splines method. CES served as the dependent variable, while ISEM indicators were treated as independent variables, with time included as a covariate. Multiple restricted cubic splines curves were fitted to explore the relationship between CES and ISEM and to identify critical thresholds. During the model fitting process, the Akaike Information Criterion (AIC) was used to evaluate the model’s performance, ensuring its reliability and goodness of fit.

(3) Analysis of variance.

Analysis of variance is a commonly employed method for testing whether significant differences exist in the mean values of a dependent variable across different categories or groups (Ding et al., 2023; Wang et al., 2022). In this study, CES was classified into five levels using the natural breaks method: low (CES1), moderately low (CES2), medium (CES3), moderately high (CES4), and high (CES5). Due to the significant scale differences between ISEM indicators, normalization was applied to ISEM to better compare the differences between groups. Analysis of variance was performed using IBM SPSS Statistics 27 to determine whether significant differences exist in ISEM variables across the different CES levels. Subsequently, the ISEM profiles for regions with different CES levels were summarized, aiming to provide theoretical guidance and practical support for regional planning within the basin.

3. Results

3.1. Spatiotemporal distribution and changes in ISEM

As shown in Fig. 3, from 2002 to 2022, NP and CA in the HRB cities exhibit a clear upward trend. The mean NP increases from 6941.37 to 7481.60, and the mean CA rises from 886.34 km<sup>2</sup> to 1292.13 km<sup>2</sup>, reflecting the continuous expansion of ISA. The mean SHAPE\_MN and mean PAFRAC increased slightly, from 1.19 to 1.20 and from 1.41 to 1.42, respectively, indicating a tiny rise in the shape and edge fractal complexity of ISA patches. Meanwhile, the mean ENN\_MN gradually decreases from 464.41 m to 366.13 m, suggesting closer distances between ISA patches, while the mean COHESION increases from 85.23 to 90.34, indicating greater spatial aggregation of ISA patches. Additionally, the magnitude of change in ISEM indicators are more pronounced from 2002 to 2012 compared to 2012 to 2022.

The spatial distribution and changes in ISEM from 2002 to 2022 are shown in Fig. 4. In terms of patch scale, high CA and NP values are primarily concentrated in cities in the central region of the Beijing-Tianjin-Hebei urban agglomeration. Specifically, high CA values are mainly observed in cities such as Beijing, Tianjin, and Baoding, while high NP values are concentrated in Baoding, Cangzhou, Tianjin, and Shijiazhuang. This indicates that these cities experience more significant ISA expansion and urbanization compared to other regions. Regarding changes, high CA increments are mainly concentrated in cities like Beijing, Tianjin, Tangshan, Baoding, and Shijiazhuang. Meanwhile, high NP increments are primarily distributed in Chengde, Zhangjiakou, Baoding, and Datong. Notably, cities such as Beijing and Tianjin even exhibit a decline in NP increments.

In terms of shape complexity, SHAPE\_MN generally follows a southeast-high and northwest-low pattern, while PAFRAC displays a north-high and south-low distribution (Fig. 4). High SHAPE\_MN values are primarily concentrated in cities such as Tangshan, Hengshui, and Dezhou, indicating greater shape complexity of ISA in these cities. In contrast, high PAFRAC values are observed in Ulanqab, Chengde, and Yangquan, reflecting more complex fractal characteristics of ISA edges in these areas. Regarding changes, SHAPE\_MN and PAFRAC exhibit relatively minor variations. From 2002 to 2012, cities like Beijing and Tianjin see declines in SHAPE\_MN, a trend that extends to more cities, including Cangzhou, Tangshan, and Hengshui, by 2022. Meanwhile, from 2002 to 2012, PAFRAC shows an upward trend in most cities across the HRB. However, by 2022, cities like Beijing, Tianjin, Zhangjiakou, and Chengde begin to exhibit declines in PAFRAC.

In terms of the spatial aggregation, ENN\_MN generally shows a northwest-high and southeast-low pattern (Fig. 4). High ENN\_MN values are primarily found in cities such as Jinzhong, Xilingol, and Chengde, indicating that ISA patches in these areas are relatively distant and scattered. Meanwhile, high COHESION values are concentrated in cities like Beijing, Tianjin, Shijiazhuang, and Xingtai, suggesting that ISA

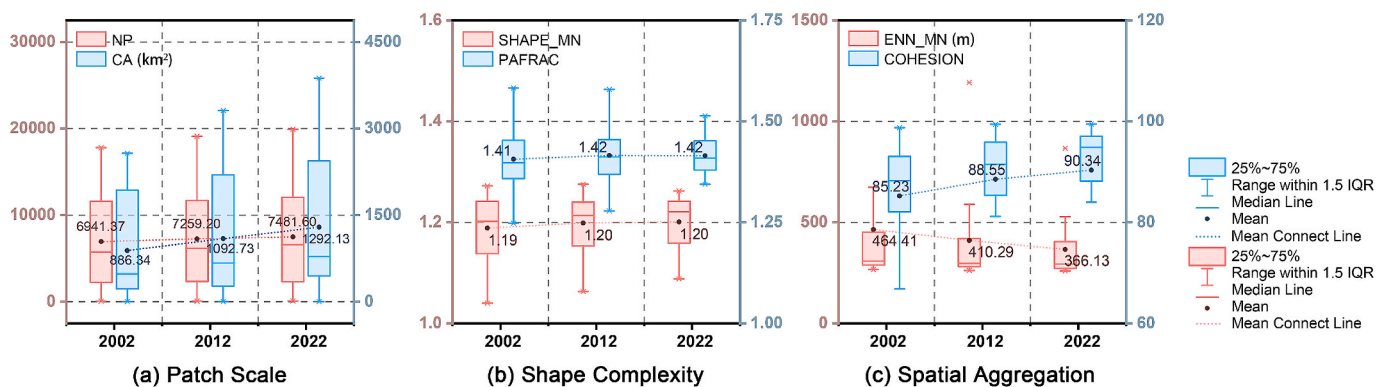


Fig. 3. Box-plots of patch scale (a), shape complexity (b), and spatial aggregation (c).

(a) Spatial Distribution

(b) Spatial Changes

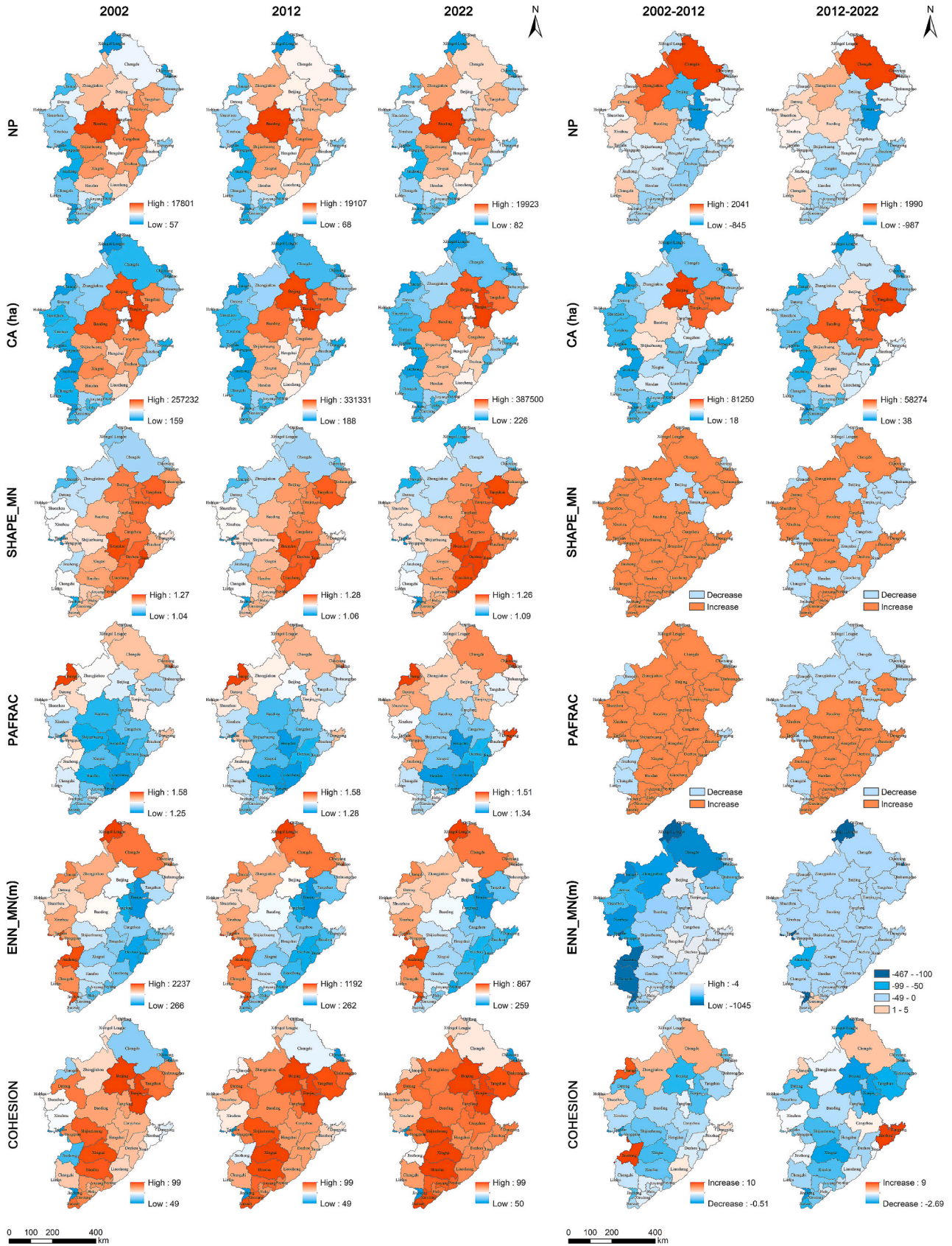


Fig. 4. Spatial distribution and changes of ISEM in HRB cities.

patches in these areas exhibit higher connectivity and integration. Regarding changes in ENN\_MN, a decline is observed across all HRB cities by 2012, with particularly notable decreases in western and northern cities such as Xilingol, Jincheng, Jinzhong, and Changzhi. By 2022, ENN\_MN values continue to decline in most cities, except for a slight increase in Xinxiang. As for COHESION changes, the most significant increments in 2012 are observed in cities such as Jinzhong, Ulanqab, Zhangjiakou, and Chengde, while by 2022, the highest increments are primarily concentrated in Dongying, Binzhou, Chengde, and Ulanqab.

### 3.2. Spatial distribution and changes in ES

#### 3.2.1. ES

As shown in Fig. 5, from 2002 to 2022, four ES exhibit an initial increase followed by a decline. Among these, water yield and soil conservation display significant variation, while habitat quality and carbon storage show smaller changes and remain relatively stable. Additionally, from 2002 to 2012, the variation in each ES indicator is more pronounced than from 2012 to 2022. From a spatial distribution perspective (Fig. 6a), habitat quality, carbon storage, and soil conservation in HRB display a pattern of lower values in the southeast and higher values in the northwest. In contrast, the spatial distribution of water yield shows dynamic changes, with high-value areas shifting from the west in 2002 to the east in 2012 and 2022.

Fig. 6b illustrates the spatial changes in ES from 2002 to 2022. For habitat quality, cities in the northwest of the HRB, such as Xilin Gol, Chengde, and Jinzhong, experience an increase in 2012 compared to 2002, while cities like Beijing, Tianjin, Langfang, and Tangshan see a slight decline. By 2022, most cities in the basin show a slight degradation of habitat quality. Regarding carbon storage, the cities that see an increase in 2012 are mostly located in the western and northern HRB, such as Jinzhong, Yangquan, and Chengde. In contrast, cities in the southeast, such as Dongying, Tianjin, and Tangshan, experience a

decrease in carbon storage. By 2022, the downward trend continues in the southeast, while carbon storage continues rising in the northwest. With respect to water yield, cities in the eastern HRB, including Tianjin, Qinhuangdao, Tangshan, and Dongying, see significant improvements in 2012 compared to 2002. In contrast, cities in the western part of the basin show only slight increases, with some even experiencing declines. By 2022, the highest increments in water yield are seen in southern cities like Binzhou, Dezhou, and Liaocheng, while water yield decreases in cities like Qinhuangdao, Tianjin, and Tangshan. Concerning soil conservation, significant improvements in 2012 are observed in northern and western cities in HRB like Qinhuangdao, Chengde, Xinzhou, and Jinzhong, while the southeastern cities show only slight increases. By 2022, the highest increments in soil conservation shift to the south, with cities like Changzhi and Anyang leading the trend, while cities such as Xinzhou, Qinhuangdao, and Zhangjiakou experience declines.

#### 3.2.2. CES

As shown in Fig. 5, from 2002 to 2022, the mean CES across HRB cities initially increases from 0.26 to 0.36, followed by a slight decline to 0.34. In terms of extreme values, the maximum CES rises from 0.70 in 2002 to 0.80 in 2022, while the minimum increases from 0.04 to 0.10, indicating improvements in both high-value and low-value regions. Overall, CES experiences a significant rise followed by a minor decline over the two decades, reflecting the phased fluctuations of CES and the persistent regional disparities.

From 2002 to 2022, CES in the HRB exhibit a spatial pattern with higher values in the southeast and lower values in the northwest (Fig. 7). High CES values are primarily concentrated in northern and western cities such as Chengde, Zhangjiakou, Qinhuangdao, and Jinzhong, while low CES values are mainly found in cities like Tianjin, Langfang, Cangzhou, and Hengshui. Between 2002 and 2012, the highest CES increments are observed in the eastern and western cities of the basin, including Qinhuangdao, Tangshan, Tianjin, and Jinzhong. In contrast, cities in the central region show smaller CES increments, with Jiaozuo

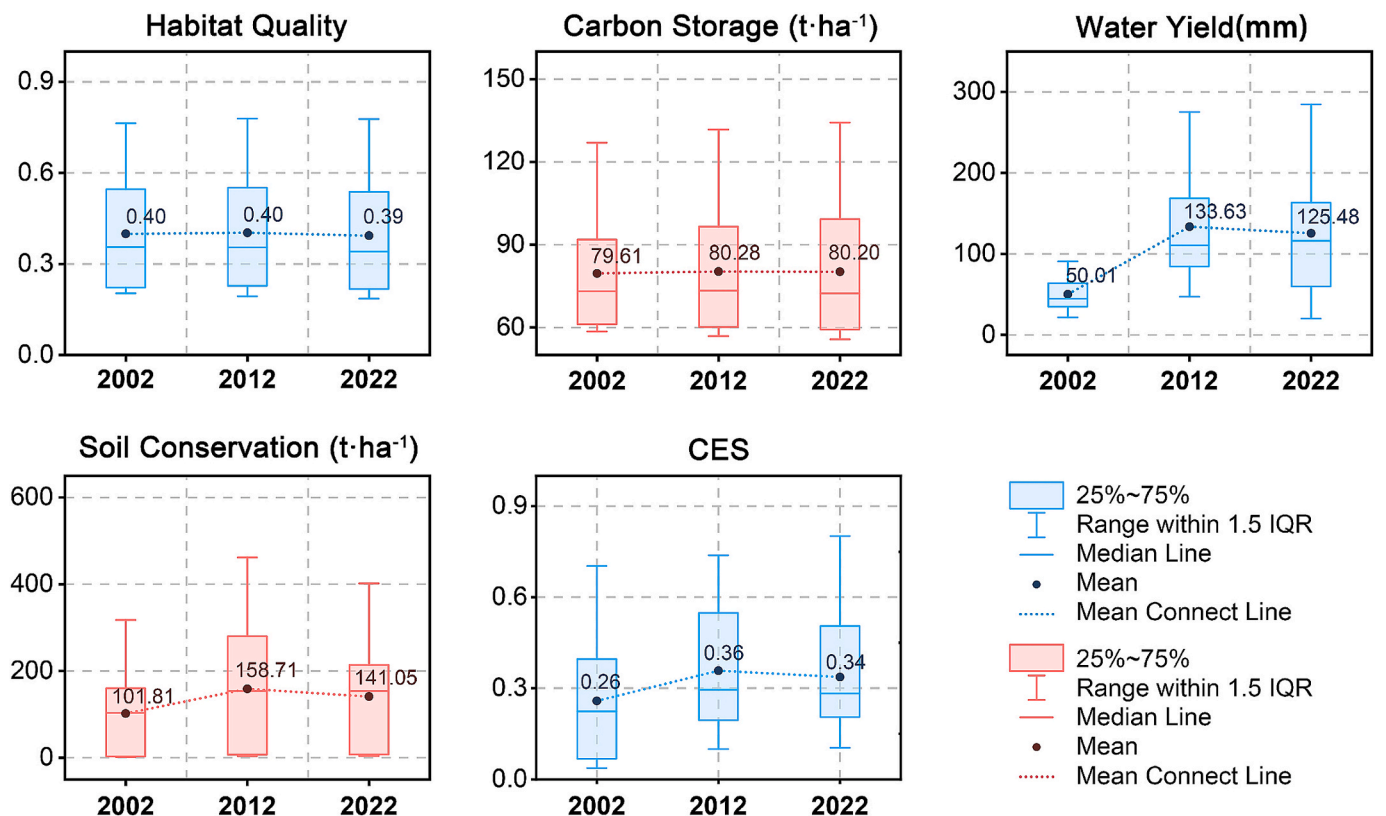


Fig. 5. Box-plots of ES and CES.

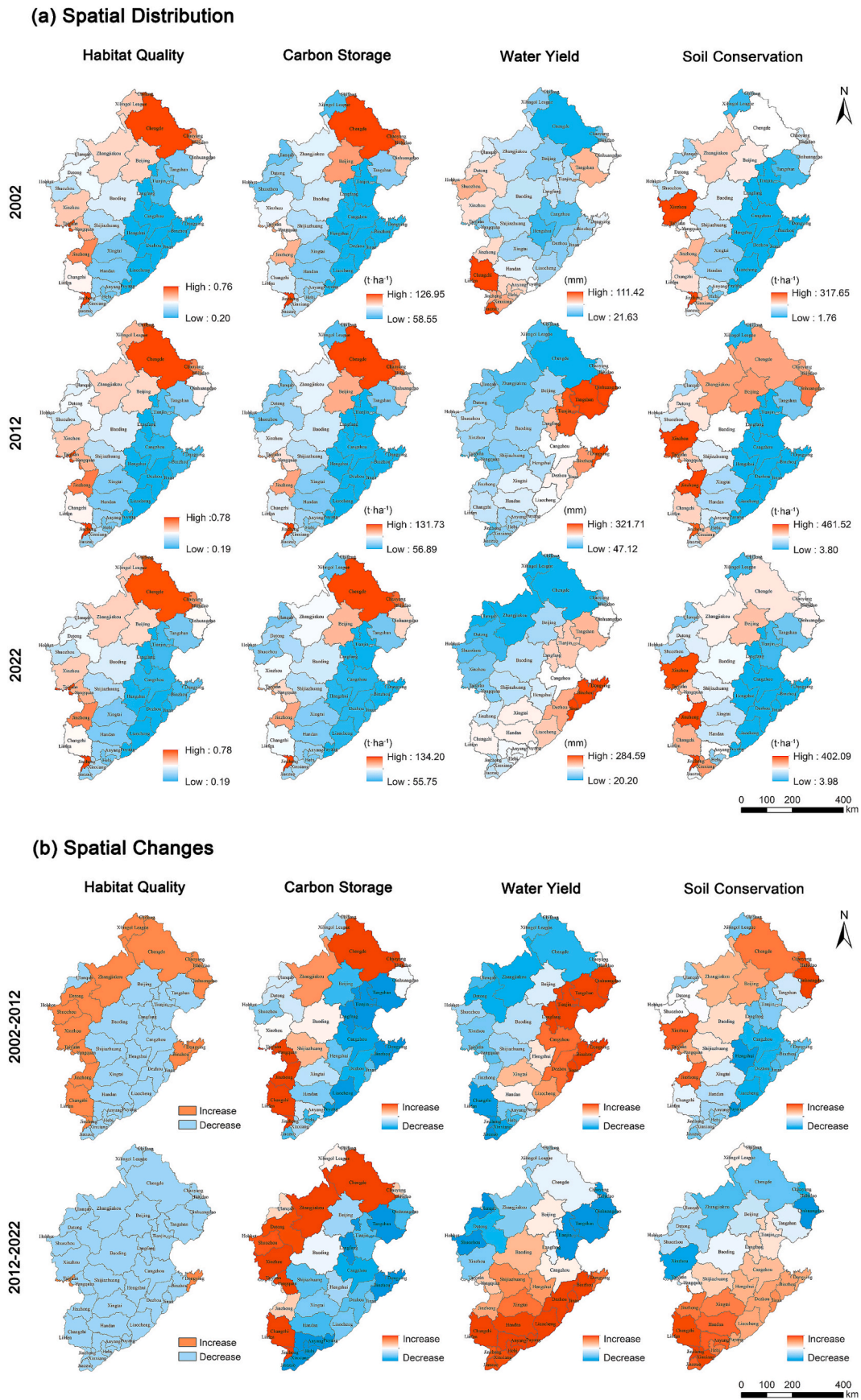
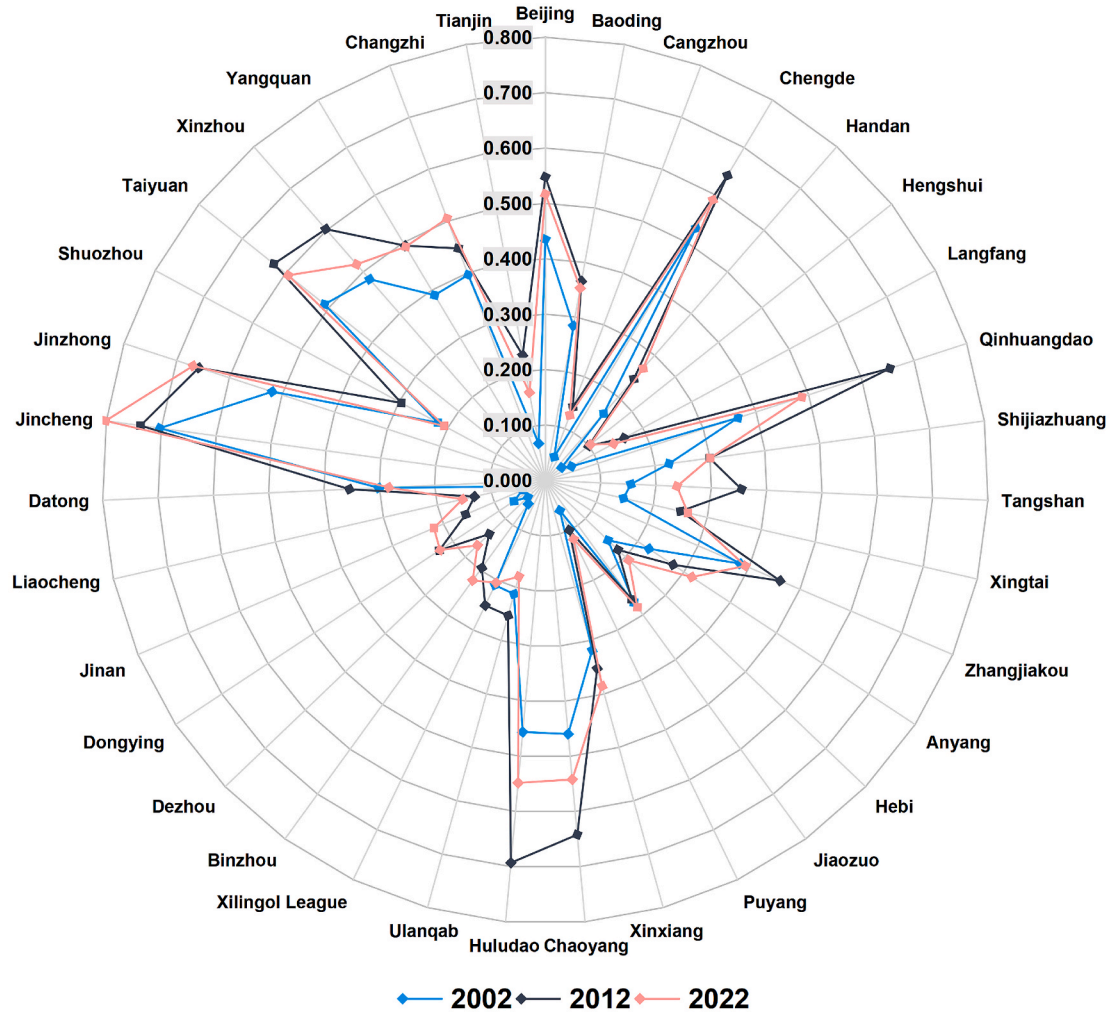


Fig. 6. Spatial distribution and changes of ES in HRB cities.

(a) CES Changes in HRB Cities



(b) Spatial Distribution and Changes

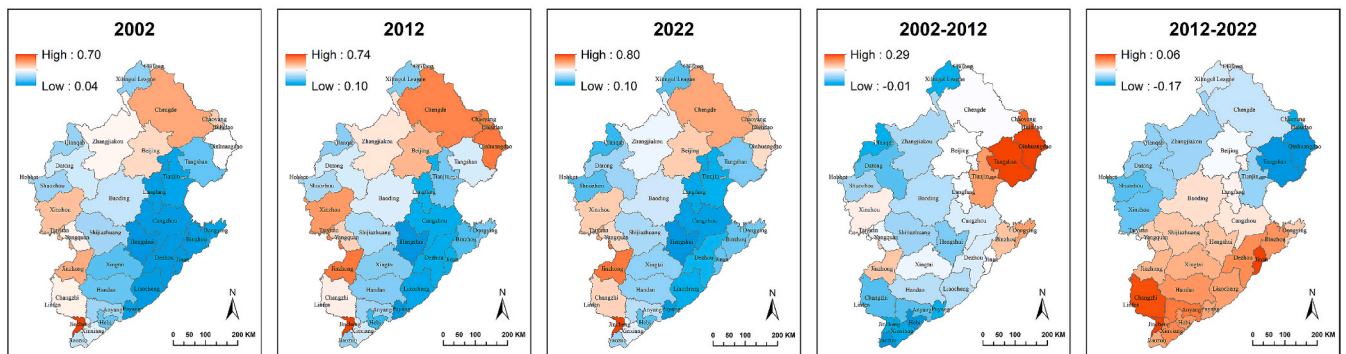


Fig. 7. CES changes (a) and spatial distribution (b).

even experiencing a decline. From 2012 to 2022, CES changes follow a pattern of lower values in the north and higher values in the south. The highest CES increments shift to cities such as Jincheng and Jinan, while cities like Qinhuangdao, Tangshan, and Tianjin see declines (Fig. 7b).

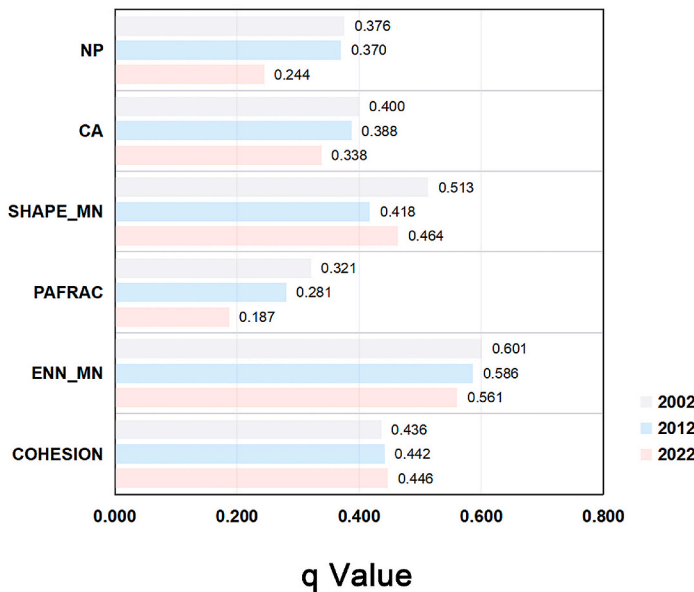
3.3. Analysis of drivers for CES

The factor detection results indicate significant changes in the drivers of CES from 2002 to 2022 (Fig. 8a). During this period, ENN\_MN, SHAPE\_MN, and COHESION are identified as the primary drivers ( $q >$

0.4). Among them, ENN\_MN demonstrates the strongest explanatory power, with  $q$ -values of 0.601, 0.586, and 0.561 in 2002, 2012, and 2022, respectively. As time progresses, the influence of ENN\_MN, NP, CA, and PAFRAC gradually decrease, while SHAPE\_MN first decrease and then increase, and COHESION show an increasing trend.

The interaction detection results (Fig. 8b) indicate that from 2002 to 2022, ISEM factors exhibit both bivariate enhancement effects and nonlinear enhancement. The combination of COHESION and SHAPE\_MN has the strongest explanatory power for CES in 2002 ( $q = 0.772$ ), ENN\_MN and PAFRAC in 2012 ( $q = 0.865$ ), and ENN\_MN and

(a) Factor Detection



(b) Interaction Factor Detection

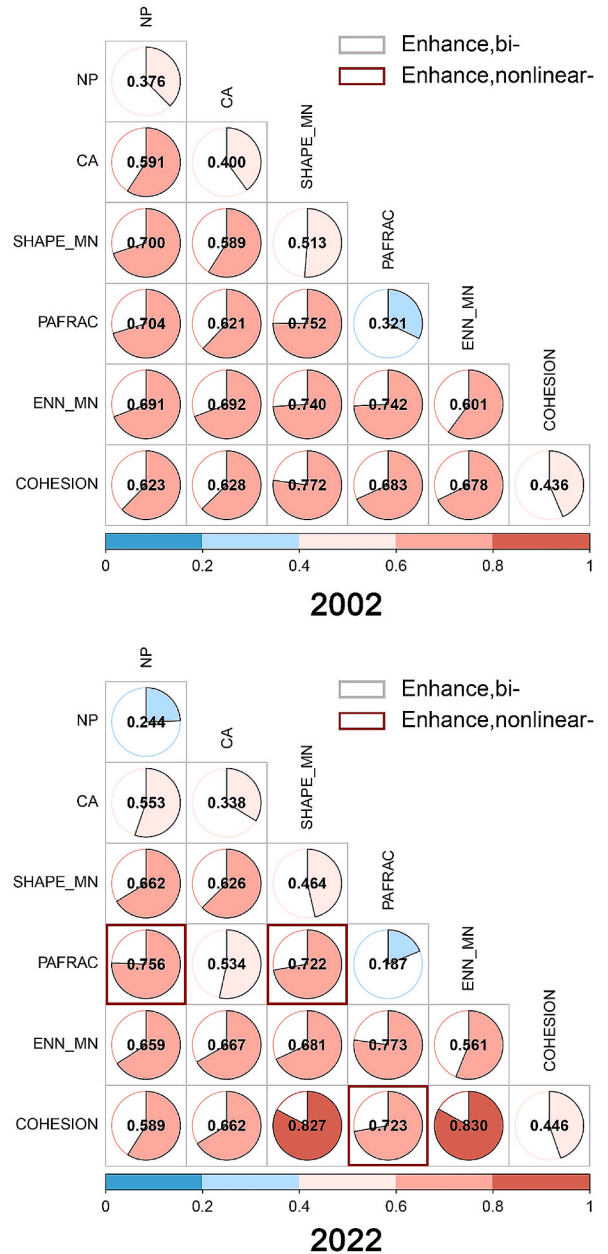


Fig. 8. Factor detection (a) and interaction detection results (b).

COHESION in 2022 ( $q = 0.830$ ). Regarding the interaction relationships between factors, in 2002, all ISEM factor combinations demonstrate bivariate enhancement, indicating that the combined influence of two factors on CES is significantly greater than the sum of their individual effects. By 2012, NP-PAFRAC and SHAPE\_MN-PAFRAC combinations show nonlinear enhancement, suggesting increasingly complex inter-factor relationships and the emergence of nonlinear influences, while other factor combinations continue to exhibit bivariate enhancement. By 2022, the nonlinear enhancement of NP-PAFRAC and SHAPE\_MN-PAFRAC persist, and the interaction between COHESION-PAFRAC transition from linear to nonlinear enhancement. This process indicates that over time, the interactions among ISEM factors gradually shift from simple dual-factor enhancement effects to more complex nonlinear enhancement effects, highlighting the dynamic and complex impacts of multi-factor interactions on ES during urban expansion.

3.4. Threshold effects of ISEM on CES

Using the restricted cubic splines, this study explores the nonlinear relationship between ISEM and CES (Fig. 9). The results indicate that, except for SHAPE\_MN ( $p > 0.05$ ), all other ISEM indicators exhibit significant nonlinear relationships with CES and have critical thresholds ( $p < 0.001$ ). When ISEM values exceed or fall below these thresholds, CES undergoes significant changes. Identifying and monitoring critical thresholds is essential for ensuring the sustainable development of ecosystems.

When the number of NP exceeds 6,599, its impact on CES begins to level off. The critical thresholds for CA and COHESION are 1,680.73 km<sup>2</sup> and 93.77, respectively, beyond which CES starts to recover. For PAFRAC, CES rapidly increases from its minimum to maximum value when PAFRAC ranges between 1.36 and 1.42, then gradually declines

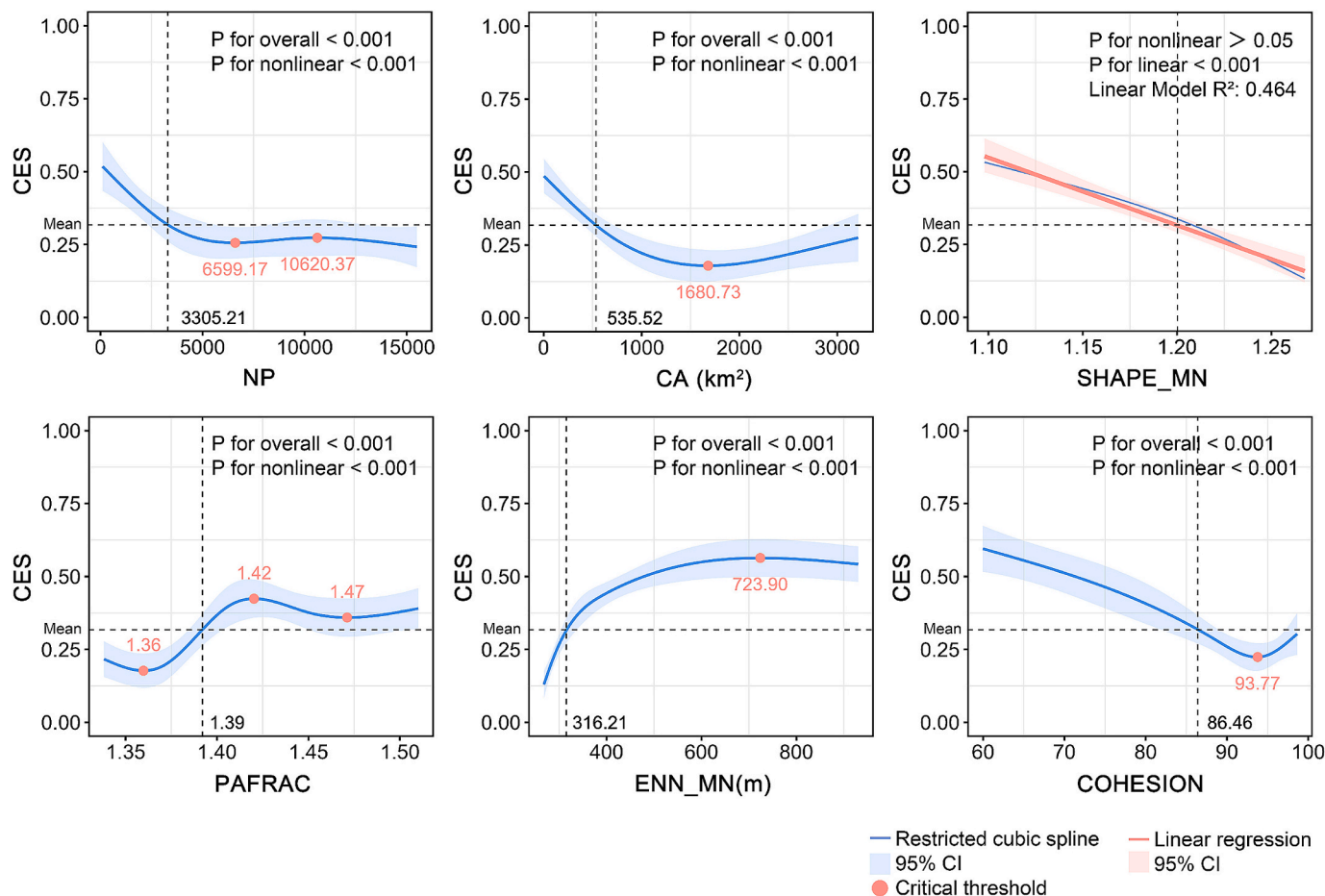


Fig. 9. Restricted cubic splines results and critical thresholds.

before rising again after 1.47. The threshold for ENN\_MN is 723.90 m, where CES peaks before starting to decline. The thresholds can serve as reference targets for landscape planning and management interventions (Li et al., 2022; Hong et al., 2024), helping to maintain the optimal state of ES in the HRB.

Additionally, when CES is at the mean level (0.32), the corresponding values for NP, CA, SHAPE\_MN, PAFRAC, ENN\_MN, and COHESION are 3,305.21, 535.52, 1.20, 1.39, 316.21, and 86.46, respectively. Based on this, combined with threshold analysis, planning ranges can be delineated for different development regions.

### 3.5. ISEM profiles across regions with different CES levels

The results (Appendix A, Table A.4) indicate significant differences ( $p < 0.01$ ) between NP, SHAPE\_MN, PAFRAC, ENN\_MN, COHESION, and CA across different CES levels. Subsequently, the ISEM profiles of regions with different CES levels were summarized (Fig. 10a), providing a scientific basis for region-specific planning.

As shown in Fig. 10a, CES5 regions, typically characterized by favorable natural and geographical conditions, exhibit the characteristics of “low NP, low CA, low SHAPE\_MN, high PAFRAC, high ENN\_MN, low COHESION.” In these regions, ISA patches are generally fewer and smaller in area, with lower shape complexity but higher fractal complexity, larger inter-patch distances, and lower aggregation levels. The ISEM in CES4 regions is characterized by “low NP, low CA, low SHAPE\_MN, high PAFRAC, moderately low ENN\_MN, high COHESION.” Compared to CES5 regions, cities in CES4 regions tend to have more ISA patches with larger areas. These patches exhibit more complex shapes and higher fractal complexity, while inter-patch distances are shorter

and aggregation levels are higher.

In CES3 regions, ISEM is characterized by “high NP, high CA, moderately high SHAPE\_MN, low PAFRAC, moderately low ENN\_MN, high COHESION.” Cities in CES3 regions generally have a higher number and larger area of ISA patches than those in CES4 and CES5 regions. The patches have more complex edges but lower fractal complexity, with higher levels of aggregation. CES1 and CES2 regions share the characteristics of “high NP, high CA, high SHAPE\_MN, low PAFRAC, low ENN\_MN, high COHESION.” Compared to CES2 regions, CES1 regions exhibit more severe fragmentation of ISA patches, with a greater number of larger patches. The patch shapes in CES1 regions tend to be more complex, but their fractal complexity is lower, and spatial aggregation levels are higher.

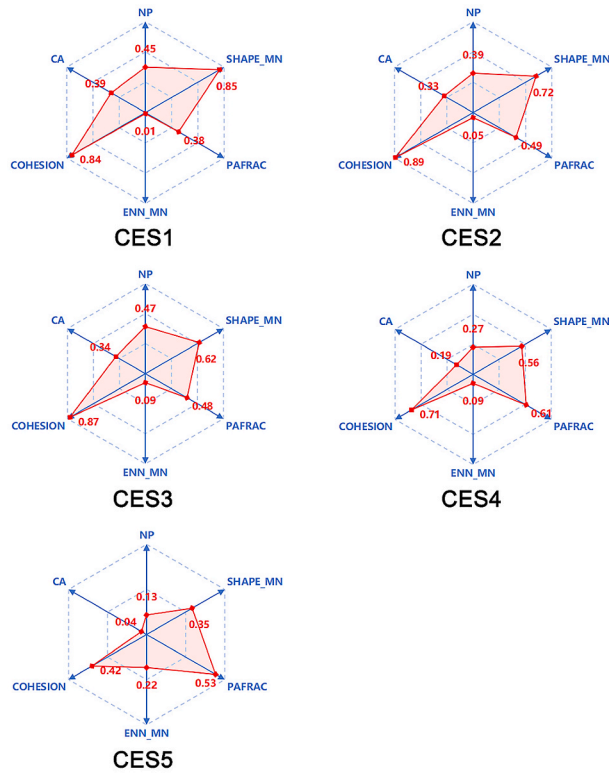
The proportions of each ISEM and their changes across regions with different CES levels are shown in Fig. 10b. From CES1 to CES5, the proportions of ENN\_MN and PAFRAC significantly increase. SHAPE\_MN shows an overall decreasing trend, though it increases in CES4. Both NP and CA generally decrease, but they show an increase in CES3. COHESION exhibits a trend of first increasing and then decreasing.

## 4. Discussion

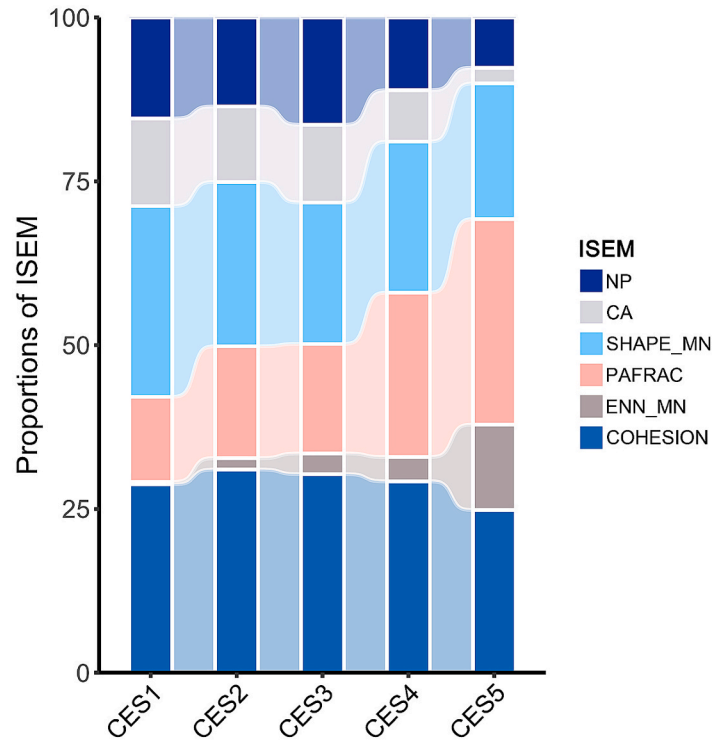
### 4.1. Impacts of planning policies on ISEM

Over the past decades, the rapid urbanization of the HRB has led to a significant increase in ISA, exerting profound impacts on basin ES. Previous studies have shown notable regional disparities in urban expansion (Liu et al., 2010), reflecting differences in urban development stages and planning strategies (Yang et al., 2018). This study reveals that

(a) ISEM Profiles



(b) Proportions of ISEM



(c) Basin Zoning Under Different CES Levels

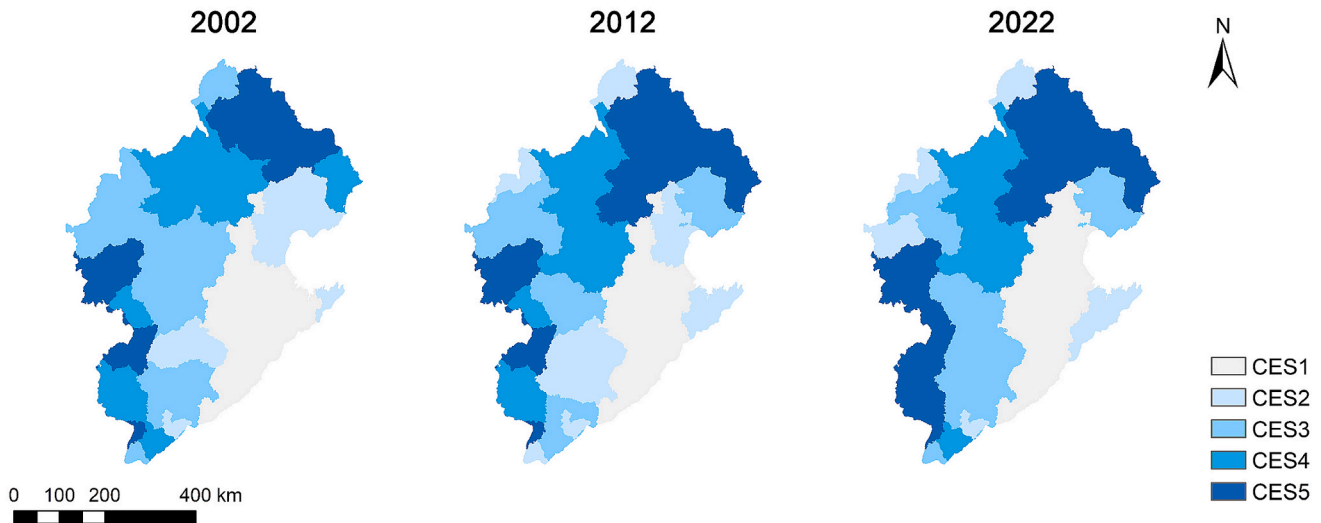


Fig. 10. ISEM profiles (a), proportions of ISEM (b), and zoning of the basin (c) for different CES levels.

the spatial distribution of ISEM in the HRB also exhibits distinct regional variations, forming a “core-periphery” differentiation pattern. Overall, the ISA patches in the Beijing-Tianjin-Hebei urban agglomeration exhibit high quantity, large area, complex shapes with smooth edges, and strong spatial aggregation, reflecting rapid urbanization and the agglomeration effect. In contrast, cities on the periphery of the HRB have fewer and smaller ISA patches with simpler shapes but more irregular edges, exhibiting a more scattered spatial distribution and a relatively lagging urbanization process. These differences have been closely linked to regional development policies (Hu et al., 2024). The

11th Five-Year Plan established urban agglomerations as the primary form of urbanization, while the 2014 elevation of Beijing-Tianjin-Hebei coordinated development to a national strategy further accelerated the expansion of the core urban agglomeration. With policy support, the development speed of the Beijing-Tianjin-Hebei urban agglomeration has continued to outpace that of other cities within the HRB.

With the phased adjustments of policies, the evolution of ISEM has also undergone significant changes. From 2012 to 2022, the expansion rate of ISA in Beijing and Tianjin slowed considerably, with a continuous decline in patch numbers, increasingly regular shapes, and enhanced

aggregation. This shift indicates a transition toward a more refined and intensive urban development model, closely linked to the urban scale control policies introduced since the 12th Five-Year Plan (Yan et al., 2015). By delineating development boundaries and optimizing land-use structures, these policies have guided the transformation of mega-city development models. During the same period, the ISA patches in Tangshan, Baoding, and Cangzhou significantly increased in area, number, and shape complexity, reflecting a shift in their functional roles within regional development. As primary recipients of Beijing’s non-capital functions and industrial relocation under the Beijing-Tianjin-Hebei coordinated development strategy, these cities have promoted urban function optimization and upgrading by accommodating industry and population transfers. Overall, the spatial distribution and evolution of ISEM in the HRB strongly reflect the guiding influence of regional development policies.

4.2. Basin planning policy recommendations based on ISEM thresholds and CES

ES are a fundamental basis for sustainable development and a key comprehensive indicator for assessing regional sustainability (Zhang et al., 2023). This study used CES levels as a criterion for delineating restricted development zones and priority conservation areas, and combined ISEM thresholds to provide decision support for ISA planning in different regions, aiming to promote sustainable development in the basin.

4.2.1. Dividing regions based on CES levels

In Section 3.5, significant differences in ISEM indicators are observed across regions with different CES levels ( $p < 0.01$ ). From a spatial distribution perspective, CES1-2 regions are primarily concentrated in plain areas, CES3 regions are mostly located in transition zones between mountains and plains, while CES4-5 regions are predominantly found in mountainous areas (Fig. 10b). This finding aligns with previous studies (Hou et al., 2022; Li et al., 2024; Ran et al., 2023). For instance, Hou et al. (2022) found that ecological risks were lower in mountainous areas and higher in plains when analyzing the impact of ISA on ecological risks in rapidly urbanizing regions.

Based on the development status and needs of regions with different levels, the CES1-3 regions can be classified as restricted development zones, while the CES4-5 regions can be designated as priority protection zones. Further subdivisions can be made within these zones into class I, class II, and general restricted development zones, as well as class I and class II priority protection zones, with differentiated management and protection measures implemented accordingly (Fig. 11). This zonal management approach not only enhances the effectiveness of ES but also promotes coordinated development within the basin, laying a foundation for regional ecological protection and sustainable development (Ding et al., 2023; Luo et al., 2024).

CES1 and CES2 regions are predominantly located in the eastern

plains of the HRB (Fig. 10b), characterized by “high NP, high CA, high SHAPE\_MN, low PAFRAC, low ENN\_MN, high COHESION.” The flat terrain facilitates rapid regional development, but the resulting high ISA coverage exacerbates ecosystem pressures (Liu et al., 2012). Consequently, these areas require more stringent management strategies to address the increasing ecological burden, while maintaining ecological balance and promoting sustainable development. Based on the development status and needs of CES1 and CES2 regions, they can be classified as class I and class II restricted development zones. The CES3 region is primarily located in the transitional zone between mountains and plains within the basin (Fig. 10b), exhibiting an ISEM profile characterized by “high NP, high CA, moderately high SHAPE\_MN, low PAFRAC, moderately low ENN\_MN, high COHESION.” This region presents a more complex ecological environment, with considerable ISA development, while also necessitating ecological protection space to balance development with ES needs. Based on the development status and needs of CES3 regions, they can be classified as general restricted development zones.

The CES4 and CES5 regions are primarily located in the northern and western parts of the basin (Fig. 10b), characterized by mountainous terrain. The ISEM profile of the CES5 region is characterized by “low NP, low CA, low SHAPE\_MN, high PAFRAC, high ENN\_MN, low COHESION,” while the CES4 region exhibits “low NP, low CA, low SHAPE\_MN, high PAFRAC, moderately low ENN\_MN, high COHESION.” Due to developmental challenges, ISA coverage in these regions is relatively low, resulting in comparatively mild ecosystem degradation (Hou et al., 2022). Overall, the CES4 and CES5 regions maintain relatively good ecological conditions, with prominent ES such as habitat quality, carbon storage, and soil conservation, making these areas highly valuable for ecological protection. Based on the development status and needs of CES5 and CES4 regions, they can be classified as class I and class II priority protection zones.

4.2.2. Multilevel CES management strategy based on ISEM thresholds

This study found that several ISEM indicators exhibit significant nonlinear relationships with CES, with CES values showing fluctuating trends of first increasing and then decreasing, or first decreasing and then increasing, as the ISEM indicators change, and with critical thresholds present. Previous studies have confirmed the existence of nonlinear relationships between urbanization and ecosystems (Chen & Chi, 2022; Ran et al., 2023; Sha et al., 2025; Zhou et al., 2018). For instance, the research by Chen & Chi (2022) revealed a U-shaped curve relationship between urbanization and CES in the urban agglomeration of the Yangtze River middle reaches. Sha et al. (2025) found that, on a macro scale, eco-environmental quality responds with an “increase-decrease-recovery” pattern as urbanization levels rise. Compared to previous studies, this study focused on the nonlinear relationships between ISA patch scale, shape complexity, and spatial aggregation, and CES. There are differences in terms of indicator construction, resulting in findings that differ from those of prior studies.

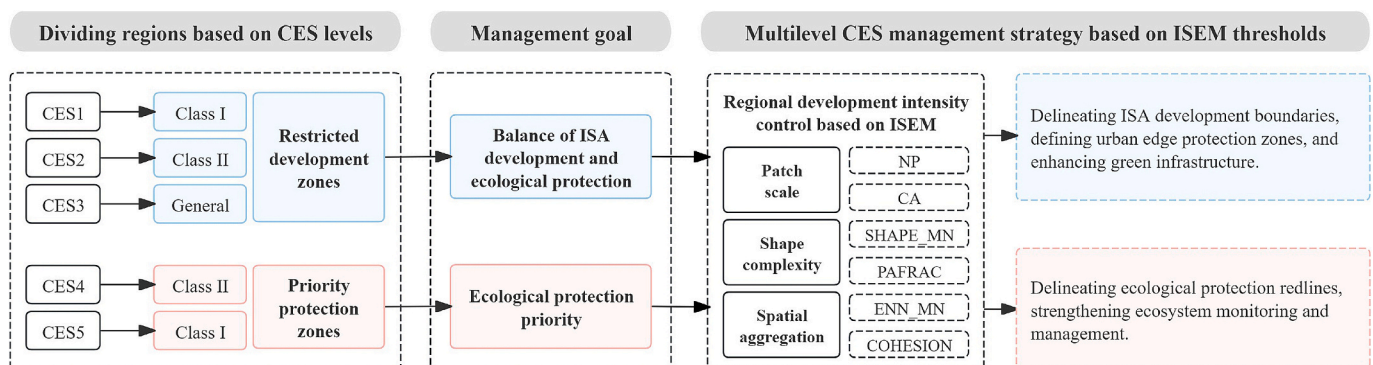


Fig. 11. Basin zoning and management based on ISEM thresholds and CES.

Based on the ISEM threshold analysis results, this study developed differentiated basin zoning management strategies (Fig. 9), aiming to achieve a dynamic balance between basin ecological protection and urban development. For the restricted development zones with a higher level of development (CES1-3), the management goal is to balance ISA development and ecological protection. NP should be controlled within the range of 6,599–10,620, CA and COHESION should be maintained above 1,680.73 km<sup>2</sup> and 93.77, respectively, and PAFRAC should be kept between 1.39 and 1.42. For specific strategies, ISEM can be effectively regulated by delineating ISA development boundaries, defining urban edge protection zones, and enhancing green infrastructure. These management strategies will support coordinated development between ISA expansion and ES, promoting more refined management and sustainable development within the basin (Zhang et al., 2023). For the less-developed regions (CES4-5), the management goal should focus on prioritizing ecological protection. To achieve this goal, NP, CA, and COHESION should be controlled below 3305.21, 535.52 km<sup>2</sup>, and 86.46, respectively, while PAFRAC should be maintained within the range of 1.39–1.42 or above 1.47. Ecological red lines can be established to prevent excessive ISA development and safeguard natural ecological functions. Additionally, ecosystem monitoring and management should be strengthened to ensure the effective maintenance and sustainable utilization of ES. For all areas within the HRB, SHAPE\_MN should be controlled below 1.2 as much as possible to avoid its adverse impact on CES. Meanwhile, ENN\_MN should be maintained within the range of 316.21–723.90 m to promote synergistic growth with CES.

Each region should flexibly adjust its management strategies based on its development stage and ISEM characteristics, in conjunction with specific target intervals. The multi-level CES basin management framework based on ISEM thresholds can not only effectively address ecological differences among regions but also optimize resource allocation and promote coordinated development of the HRB.

#### 4.3. Limitations

The proposed planning framework provides differentiated development and protection strategies for regions with different CES levels within the basin. However, it is important to note that the influence of ISEM on CES may vary across different basins and regions. Due to limitations in the relevant data and the geographical characteristics of the study area, the findings of this study may need to be adjusted when applied to other regions to avoid potential biases. In practical planning, it is essential to consider the specific circumstances of each region and other policy requirements to ensure the feasibility and effectiveness of the proposed plans.

#### 5. Conclusions

This study, using the HRB as a case, constructed a basin planning framework based on CES zoning and ISEM thresholds, and explored the nonlinear relationships between ISEM and CES. The results showed that ISEM indicators significantly influenced CES, with interactions characterized by bivariate or nonlinear enhancement. Over time, the number of nonlinear enhancement combinations increased, revealing the complexity of their interactions. Additionally, significant differences in NP, SHAPE\_MN, PAFRAC, ENN\_MN, COHESION, and CA were observed across CES samples, particularly in areas with high and low CES levels, where ISEM exhibited contrasting differences. Thus, CES levels were proposed as a basis for delineating restricted development zones and priority protected zones, providing scientific guidance for regional ecological conservation and development. Notably, except for SHAPE\_MN, all ISEM Indicators exhibited significant nonlinear relationships and critical thresholds with CES. Exceeding these thresholds will lead to significant changes in CES, providing quantitative reference point for the planning and management of ISA in basin.

Against the backdrop of rapid global urbanization and intensifying

climate change, the framework proposed in this study provides a scientific decision-support tool for coordinating ecological conservation and urban development, offering significant academic value and broad application prospects. Future research could further expand the framework's applicability to diverse geographical environments and incorporate additional dimensions of variables, thereby providing a more robust scientific foundation for global sustainable development.

#### CRedit authorship contribution statement

**Yang Gu:** Writing – review & editing, Writing – original draft, Visualization, Validation, Software, Methodology, Investigation, Formal analysis, Data curation, Conceptualization. **Yujia Chen:** Writing – review & editing, Visualization, Validation, Software, Formal analysis, Data curation. **Dongdong Yang:** Supervision, Resources, Project administration, Funding acquisition, Conceptualization. **Xin Zhao:** Supervision, Methodology, Conceptualization. **Shunqi Pan:** Supervision, Resources, Project administration.

#### Funding

This work was supported by National Natural Science Foundation of China (Grant No. 52078326).

#### Declaration of competing interest

The authors declare that they have no known competing financial interests or personal relationships that could have appeared to influence the work reported in this paper.

#### Appendix A. Supplementary data

Supplementary data to this article can be found online at <https://doi.org/10.1016/j.ecolind.2025.113493>.

#### Data availability

Data will be made available on request.

#### References

- Bhaskaran, K., dos-Santos-Silva, I., Leon, D.A., Douglas, I.J., Smeeth, L., 2018. Association of BMI with overall and cause-specific mortality: a population-based cohort study of 3.6 million adults in the UK. *Lancet*. *Endocrinol.* 6 (12), 944–953. [https://doi.org/10.1016/s2213-8587\(18\)30288-2](https://doi.org/10.1016/s2213-8587(18)30288-2).
- Bin, L.L., Xu, K., Yang, Z.W., He, L., Xu, X.Y., Lian, J.J., 2024. Water cycle evolution in the Haihe River Basin and its relationship with landscape pattern changes. *Ecol. Ind.* 159 (13), 111681. <https://doi.org/10.1016/j.ecolind.2024.111681>.
- Chen, G.Z., Li, X., Liu, X.P., Chen, Y.M., Liang, X., Leng, J.Y., Xu, X.C., Liao, W.L., Qiu, Y. A., Wu, Q.L., Huang, K.N., 2020. Global projections of future urban land expansion under shared socioeconomic pathways. *Nat. Commun.* 11 (1), 12. <https://doi.org/10.1038/s41467-020-14386-x>. Article 537.
- Chen, W.X., Chi, G.Q., 2022. Urbanization and ecosystem services: The multi-scale spatial spillover effects and spatial variations. *Land Use Policy* 114 (14), 105964. <https://doi.org/10.1016/j.landusepol.2021.105964>.
- Cord, A.F., Bartkowski, B., Beckmann, M., Ditttrich, A., Hermans-Neumann, K., Kaim, A., Lienhoop, N., Locher-Krause, K., Priess, J., Schröter-Schlaack, C., Schwarz, N., Seppelt, R., Strauch, M., Václavík, T., Volk, M., 2017. Towards systematic analyses of ecosystem service trade-offs and synergies: Main concepts, methods and the road ahead. *Ecosyst. Serv.* 28, 264–272. <https://doi.org/10.1016/j.ecoser.2017.07.012>.
- Costanza, R., D'Arge, R., De Groot, R., Farber, S., Grasso, M., Hannon, B., Limburg, K., Naeem, S., O'Neill, R.V., Paruelo, J., Raskin, R.G., Sutton, P., Van Den Belt, M., 1997. The value of the world's ecosystem services and natural capital. *Nature* 387 (6630), 253–260. <https://doi.org/10.1038/387253a0>.
- Dahlgren, J.P., García, M.B., Ehrlén, J., 2011. Nonlinear relationships between vital rates and state variables in demographic models. *Ecology* 92 (5), 1181–1187. <https://doi.org/10.1890/10-1184.1>.
- Deng, C.B., Zhu, Z., 2020. Continuous subpixel monitoring of urban impervious surface using Landsat time series. *Remote Sens. Environ.* 238 (21), 110929. <https://doi.org/10.1016/j.rse.2018.10.011>.
- Deng, Y., Shao, Z., Dang, C., Huang, X., Zhuang, Q., 2023. The impact of policies on land cover and ecosystem services dynamics in the Poyang Lake Ecological Economic

- Zone, China. *Ecol. Indic.* 156, 111169. <https://doi.org/10.1016/j.ecolind.2023.111169>.
- Ding, T.H., Chen, J.F., Fang, Z., Chen, J.Y., 2021. Assessment of coordinative relationship between comprehensive ecosystem service and urbanization: A case study of Yangtze River Delta urban Agglomerations, China. *Ecol. Indic.* 133 (15), 108454. <https://doi.org/10.1016/j.ecolind.2021.108454>.
- Ding, T.H., Chen, J.F., Fang, Z., Wang, Y., 2023. Exploring the differences of ecosystem service values in different functional areas of metropolitan areas. *Sustain. Prod. Consumpt.* 38, 341–355. <https://doi.org/10.1016/j.spc.2023.04.016>.
- Fang, Z., Xue, S., Zhou, Q., Cheng, C.G., Bai, Y., Huang, Z.D., Wang, J., Wang, R.B., Wang, Y.X., Wu, R., Rong, J., Hong, J., Ding, T.H., 2024. Unveiling driving disparities between satisfaction and equity of ecosystem services in urbanized areas. *Resour. Environ. Sustainability* 18 (16), 100176. <https://doi.org/10.1016/j.resenv.2024.100176>.
- Gong, P., Li, X.C., Wang, J., Bai, Y.Q., Cheng, B., Hu, T.Y., Liu, X.P., Xu, B., Yang, J., Zhang, W., Zhou, Y.Y., 2020. Annual maps of global artificial impervious area (GAI) between 1985 and 2018. *Remote Sens. Environ.* 236 (12), 111510. <https://doi.org/10.1016/j.rse.2019.111510>.
- Gui, B.L., Bhardwaj, A., Sam, L., 2024. Revealing the evolution of spatiotemporal patterns of urban expansion using mathematical modelling and emerging hotspot analysis. *J. Environ. Manage.* 364 (22), 121477. <https://doi.org/10.1016/j.jenvman.2024.121477>.
- He, J., Yang, X.H., Li, J.Q., Jin, J.L., Wei, Y.M., Chen, X.J., 2015. Spatiotemporal variation of meteorological droughts based on the daily comprehensive drought index in the Haihe River basin, China. *Nat. Hazards* 75, S199–S217. <https://doi.org/10.1007/s11069-014-1158-8>.
- He, M.X., Xu, J., Xiao, Y., Gu, X.T., Pang, Q., Zhou, Y., Xie, G.D., 2025. A systematic review of the progress of research on comprehensive benefit assessment of national-level ecological protection projects in China. *Environ. Impact Assess. Rev.* 112 (20), 107816. <https://doi.org/10.1016/j.eiar.2025.107816>.
- Hong, G., Liu, S.J., Liu, W.P., Wu, X.F., 2024. Nonlinear trade-off relationship and critical threshold between ecosystem services and climate resilience for sustainable urban development. *Sustain. Cities Soc.* 103 (18), 105253. <https://doi.org/10.1016/j.scs.2024.105253>.
- Hou, L., Wu, F.Q., Xie, X.L., 2020. The spatial characteristics and relationships between landscape pattern and ecosystem service value along an urban-rural gradient in Xi'an city, China. *Ecol. Indic.* 108 (10), 105720. <https://doi.org/10.1016/j.ecolind.2019.105720>.
- Hou, Y., Ding, W.H., Liu, C.F., Li, K., Cui, H.T., Liu, B.Y., Chen, W.P., 2022. Influences of impervious surfaces on ecological risks and controlling strategies in rapidly urbanizing regions. *Sci. Total Environ.* 825 (12), 153823. <https://doi.org/10.1016/j.scitotenv.2022.153823>.
- Hu, Y.N., Connor, D.S., Stuhlmacher, M., Peng, J., Turner II, B.L.T., 2024. More urbanization, more polarization: evidence from two decades of urban expansion in China. *Npj Urban Sustain.* 4 (1), 11. <https://doi.org/10.1038/s42949-024-00170-z>.
- Li, D.L., Cao, W.F., Dou, Y.H., Wu, S.Y., Liu, J.G., Li, S.C., 2022. Non-linear effects of natural and anthropogenic drivers on ecosystem services: Integrating thresholds into conservation planning. *J. Environ. Manage.* 321 (11), 116047. <https://doi.org/10.1016/j.jenvman.2022.116047>.
- Li, L.N., Liu, Y.S., 2019. Spatial-temporal patterns and driving forces of sustainable urbanization in China Since 2000. Article 05019014 *J. Urban Plann. Dev.* 145 (4). [https://doi.org/10.1061/\(asce\)jup.1943-5444.0000528](https://doi.org/10.1061/(asce)jup.1943-5444.0000528).
- Li, Q., Li, D., Wang, J.F., Wang, S., Wang, R.D., Fu, G., Yuan, Y.X., Zheng, Z.H., 2024. Spatial heterogeneity of ecosystem service bundles and the driving factors in the Beijing-Tianjin-Hebei region. *J. Clean. Prod.* 479, 144006. <https://doi.org/10.1016/j.jclepro.2024.144006>.
- Ling, M., Guo, X., Shi, X., Han, H., 2022. Temporal and spatial evolution of drought in Haihe River Basin from 1960 to 2020. *Ecol. Ind.* 138, 108809. <https://doi.org/10.1016/j.ecolind.2022.108809>.
- Liu, J.Y., Zhang, Z.X., Xu, X.L., Kuang, W.H., Zhou, W.C., Zhang, S.W., Li, R.D., Yan, C.Z., Yu, D.S., Wu, S.X., Nan, J., 2010. Spatial patterns and driving forces of land use change in China during the early 21st century. *J. Geog. Sci.* 20 (4), 483–494. <https://doi.org/10.1007/s11442-010-0483-4>.
- Liu, Q., Tian, H., Yang, Y., 2012. Quantitative study of the relationship between the distribution of cities and the natural environment based on GIS and RS in China. *Sci. Geogr. Sin.* 32 (6), 686–693.
- Liu, X.P., Huang, Y.H., Xu, X.C., Li, X.C., Li, X., Ciais, P., Lin, P.R., Gong, K., Ziegler, A.D., Chen, A.N., Gong, P., Chen, J., Hu, G.H., Chen, Y.M., Wang, S.J., Wu, Q.S., Huang, K. N., Estes, L., Zeng, Z.Z., 2020. High-spatiotemporal-resolution mapping of global urban land change from 1985 to 2015. *Nat. Sustain.* 3 (7), 564. <https://doi.org/10.1038/s41893-020-0521-x>.
- Livina, V.N., Lenton, T.M., 2007. A modified method for detecting incipient bifurcations in a dynamical system. *Geophys. Res. Lett.* 34 (3). <https://doi.org/10.1029/2006gl028672>. Article L03712.
- Luo, K., Wang, H.W., Yan, X.M., Ma, C., Zheng, X.D., Wu, J.H., Wu, C.R., 2024. Study on trade-offs and synergies of rural ecosystem services in the Tacheng-Emin Basin, Xinjiang, China: Implications for zoning management of rural ecological functions. *J. Environ. Manage.* 363 (17), 121411. <https://doi.org/10.1016/j.jenvman.2024.121411>.
- Ma, Y., Zhang, S., Yang, K., Li, M., 2021. Influence of spatiotemporal pattern changes of impervious surface of urban megaregion on thermal environment: A case study of the Guangdong - Hong Kong - Macao Greater Bay Area of China. *Ecol. Ind.* 121, 107106. <https://doi.org/10.1016/j.ecolind.2020.107106>.
- Mao, D., He, X., Wang, Z., Tian, Y., Xiang, H., Yu, H., Man, W., Jia, M., Ren, C., Zheng, H., 2019. Diverse policies leading to contrasting impacts on land cover and ecosystem services in Northeast China. *J. Clean. Prod.* 240, 117961. <https://doi.org/10.1016/j.jclepro.2019.117961>.
- Ministry of Ecology and Environment, PRC. (2023). Water ecological environment protection plan for key river basins. [https://www.mee.gov.cn/zcwj/zcjd/202306/t20230605\\_1032610.shtml](https://www.mee.gov.cn/zcwj/zcjd/202306/t20230605_1032610.shtml).
- National Development and Reform Commission. (2021). 14th Five-Year Plan for comprehensive treatment of water environment in key river basins. <https://www.ndrc.gov.cn/xxgk/zcfb/ghwb/202201/P020220111669050733286.pdf>.
- Peng, J., Tian, L., Liu, Y., Zhao, M., Hu, Y.N., Wu, J., 2017. Ecosystem services response to urbanization in metropolitan areas: Thresholds identification. *Sci. Total Environ.* 607, 706–714. <https://doi.org/10.1016/j.scitotenv.2017.06.218>.
- Qiu, L.H., He, J.H., Yue, C., Ciais, P., Zheng, C.M., 2024. Substantial terrestrial carbon emissions from global expansion of impervious surface area. *Nat. Commun.* 15 (1), 13. <https://doi.org/10.1038/s41467-024-50840-w>. Article 6456.
- Ran, Z., Gao, S., Zhang, B.F., Guo, C.Y., Ouyang, X., Gao, J.H., 2023. Non-linear effects of multi-dimensional urbanization on ecosystem services in mega-urban agglomerations and its threshold identification. *Ecol. Ind.* 154 (14), 110846. <https://doi.org/10.1016/j.ecolind.2023.110846>.
- Reader, M.O., Eppinga, M.B., de Boer, H.J., Damm, A., Petchey, O.L., Santos, M.J., 2022. The relationship between ecosystem services and human modification displays decoupling across global delta systems (vol 3, 102, 2022) [Correction]. *Commun. Earth Environ.* 3 (1), 1. <https://doi.org/10.1038/s43247-022-00449-y>. Article 115.
- Ren, Q., He, C.Y., Huang, Q.X., Shi, P.J., Zhang, D., Güneralp, B., 2022. Impacts of urban expansion on natural habitats in global drylands. *Nat. Sustain.* 5 (10), 869–878. <https://doi.org/10.1038/s41893-022-00930-8>.
- Ren, Y.F., Zhang, L.B., Wei, X.X., Song, Y., Wu, S.Y., Wang, H., Chen, X., Qiao, Y.B., Liang, T., 2024. Evaluating and simulating the impact of afforestation policy on land use and ecosystem services trade-offs in Linyi, China. *Ecol. Ind.* 160 (15), 111898. <https://doi.org/10.1016/j.ecolind.2024.111898>.
- Samuel, E.M., Mitchell, R.M., Winkler, D.E., 2023. Perspectives on challenges and opportunities at the restoration-policy interface in the USA. *Restor. Ecol.* 31 (4), 9. <https://doi.org/10.1111/rec.13823>.
- Scheffer, M., Hirota, M., Holmgren, M., Van Nes, E.H., Chapin III, F.S., 2012. Thresholds for boreal biome transitions. *PNAS* 109 (52), 21384–21389. <https://doi.org/10.1073/pnas.1219844110>.
- Sha, A.M., Zhang, J.J., Pan, Y.J., Zhang, S.G., 2025. How to recognize and measure the impact of phasing urbanization on eco-environment quality: An empirical case study of 19 urban agglomerations in China. *Technol. Forecast. Soc. Chang.* 210 (15), 123845. <https://doi.org/10.1016/j.techfore.2024.123845>.
- Wang, J., Wu, S., Wang, Y., Yan, D., Cheng, M., Zhou, W., Liu, Z., 2024. Spatiotemporal decoupling between impervious surface areas and ecosystem services. *Environ. Sci. Pollut. Res.* 31 (3), 3707–3721. <https://doi.org/10.1007/s11356-023-31201-4>.
- Wang, J., Xu, C., 2017. Geodetector: Principle and prospective. *Acta Geograph. Sin.* 72 (1), 116–134.
- Wang, J., Zhou, W., Guan, Y.J., 2022. Optimization of management by analyzing ecosystem service value variations in different watersheds in the Three-River Headwaters Basin. *J. Environ. Manage.* 321 (12), 115956. <https://doi.org/10.1016/j.jenvman.2022.115956>.
- Wang, Z.-G., Luo, Y.-Z., Zhang, M.-H., Xia, J., 2014. Quantitative evaluation of sustainable development and eco-environmental carrying capacity in water-deficient regions: A case study in the Haihe River Basin, China. *J. Integ. Agricul.* 13 (1), 195–206. [https://doi.org/10.1016/s2095-3119\(13\)60423-2](https://doi.org/10.1016/s2095-3119(13)60423-2).
- Xia, H., Yuan, S.F., Prishchepov, A.V., 2023. Spatial-temporal heterogeneity of ecosystem service interactions and their social-ecological drivers: Implications for spatial planning and management. *Resour. Conserv. Recycl.* 189 (16), 106767. <https://doi.org/10.1016/j.resconrec.2022.106767>.
- Xiao, R., Lin, M., Fei, X.F., Li, Y.S., Zhang, Z.H., Meng, Q.X., 2020. Exploring the interactive coercing relationship between urbanization and ecosystem service value in the Shanghai-Hangzhou Bay Metropolitan Region. *J. Clean. Prod.* 253, 119803. <https://doi.org/10.1016/j.jclepro.2019.119803>.
- Xu, H., Li, C., Hu, Y., Li, S., Kong, R., Zhang, Z., 2023. Quantifying the effects of 2D/3D urban landscape patterns on land surface temperature: A perspective from cities of different sizes. *Build. Environ.* 233, 110085. <https://doi.org/10.1016/j.buildenv.2023.110085>.
- Xu, X., Yang, D., Yang, H., Lei, H., 2014. Attribution analysis based on the Budyko hypothesis for detecting the dominant cause of runoff decline in Haihe basin. *J. Hydrol.* 510, 530–540. <https://doi.org/10.1016/j.jhydrol.2013.12.052>.
- Yan, J.M., Xia, F.Z., Bao, H.X.H., 2015. Strategic planning framework for land consolidation in China: A top-level design based on SWOT analysis. *Habitat Int.* 48, 46–54. <https://doi.org/10.1016/j.habitatint.2015.03.001>.
- Yang, J., Huang, X., 2021. The 30 m annual land cover dataset and its dynamics in China from 1990 to 2019. *Earth Syst. Sci. Data* 13 (8), 3907–3925. <https://doi.org/10.5194/essd-13-3907-2021>.
- Yang, Y., Yuan, X.F., An, J.J., Su, Q.J., Chen, B., 2024. Drivers of ecosystem services and their trade-offs and synergies in different land use policy zones of Shaanxi Province, China. *J. Cleaner Product.* 452 (15), 142077. <https://doi.org/10.1016/j.jclepro.2024.142077>.
- Yang, Y.Y., Liu, Y.S., Li, Y.R., Du, G.M., 2018. Quantifying spatio-temporal patterns of urban expansion in Beijing during 1985-2013 with rural-urban development transformation. *Land Use Policy* 74, 220–230. <https://doi.org/10.1016/j.landusepol.2017.07.004>.
- Zhang, H.J., Zhang, Z.C., Liu, K., Huang, C.B., Dong, G.P., 2023. Integrating land use management with trade-offs between ecosystem services: A framework and application. *Ecol. Ind.* 149 (13), 110193. <https://doi.org/10.1016/j.ecolind.2023.110193>.

- Zhang, Z.M., Peng, J., Xu, Z.H., Wang, X.Y., Meersmans, J., 2021. Ecosystem services supply and demand response to urbanization: A case study of the Pearl River Delta, China. *Ecosystem Services* 49, 101274. <https://doi.org/10.1016/j.ecoser.2021.101274>.
- Zheng, Y., Fan, Y., Ji, J.Y., Jia, C.G., Luo, K.Y., Wei, C.X., Song, Y.T., 2024. The relationship between basin urbanization and ecosystem services in China: a case study of Central China (CC) urban agglomeration. *Urban Ecosystems* 27 (4), 993–1010. <https://doi.org/10.1007/s11252-023-01496-9>.
- Zhong, J., Jiao, L.M., Droin, A., Liu, J.F., Lian, X.H., Taubenbo, H., 2023. Greener cities cost more green: Examining the impacts of different urban expansion patterns on NPP. *Build. Environ.* 228 (12), 109876. <https://doi.org/10.1016/j.buildenv.2022.109876>.
- Zhou, D.Y., Tian, Y.Y., Jiang, G.H., 2018. Spatio-temporal investigation of the interactive relationship between urbanization and ecosystem services: Case study of the Jingjinji urban agglomeration, China. *Ecol. Ind.* 95, 152–164. <https://doi.org/10.1016/j.ecolind.2018.07.007>.